ELSEVIER

Fire Safety Journal 33 (1999) 167–184

FIRE SAFETY JOURNAL

www.elsevier.com/locate/firesaf

Quantifying fire model evaluation using functional analysis

Richard D. Peacock*, Paul A. Reneke, William D. Davis, Walter W. Jones

Building and Fire Research Laboratory, National Institute of Standards and Technology, Gaithersburg, MD 20899-8642, USA

Received 9 May 1999; accepted 14 June 1999

Abstract

Comparisons of predictive fire models with each other or with experimental data have been largely qualitative. By treating these time series curves as infinite-dimensional vectors, a branch of mathematics called functional analysis defines geometrically meaningful operations on the curves. This allows lengths, angles, and distance between two arbitrary curves to be defined and quantified. An introduction to the theory and tools provided by functional analysis is presented. Examples of the application of these tools to fire model evaluation are presented. Published by Elsevier Science Ltd. All rights reserved.

1. Introduction and background

The ASTM guide for evaluating the predictive capability of fire models [1] identifies four areas important for fire model evaluation: (1) model and scenario definition, (2) theoretical basis and assumptions in the model, (3) mathematical and numerical robustness of the model, and (4) quantifying the uncertainty and accuracy of the model. The first two of these are largely documentation and policy issues. Additional guidance is available in the ASTM guide for fire model documentation [2]. The work of Forney [3] examines the mathematical robustness of fire models using the CFAST model as an example. Sensitivity analysis and fire model comparisons are the primary focus of the final area. Key to both sensitivity analysis and fire model comparisons

* Corresponding author. Fax: 001-301-975-4052.
E-mail address: moogle@nist.gov (R.D. Peacock)

0379-7112/99/$ - see front matter.
PII: S0379-7112(99)00029-6

is the ability to quantify the difference between model predictions and experimental measurements or between two sets of model predictions or experimental measurements. This paper examines techniques for quantifying these comparisons. These techniques are of use in comparing models and experiments, comparing models to one another, and comparing model predictions with sensor data for use in fire detection and prediction in real-time systems.

A number of researchers have studied the level of agreement between computer fire models and real-scale fires. These comparisons fall into two broad categories: fire reconstruction and comparison with laboratory experiments. Both categories provide a level of verification for the models used. Fire reconstruction, although often more qualitative, provides a higher degree of confidence for the user when the models successfully simulate real-life conditions. Comparisons with laboratory experiments, however, can yield detailed comparisons that point out weaknesses in the individual phenomena included in the models. The latter is also used for deciding what improvements need to be made. Some of the comparisons in the literature are reviewed below. Nelson [4] used simple computer fire models along with existing experimental data to develop an analysis of a large high-rise building fire. This analysis showed the value of available analytical calculations in reconstructing the events involved in a multiple-story fire. Bukowski [5–7] has applied the FAST and CFAST models in several fatal fire reconstructions. Details of the fires including temperatures, vent flows, and gas concentrations were consistent with observed conditions and witness accounts. Emmons [8] applied computer fire modeling to the MGM Grand Hotel fire of 1980. Using the HARVARD 5 model, he analyzed the relative contributions of booth seating, ceiling tiles, decorative beams, and the HVAC system on the outcome of the fire.

Several additional studies comparing model predictions with experimental measurements are available. Mitler and Rockett [9] utilized the Harvard Computer Fire Code V to model two in a series of eight well-instrumented full-scale room fires. They reported "good to excellent" agreement for most of the model variables studied. Rockett, Morita, and Cooper [10] used the HARVARD VI multi-room fire model to simulate the results of real-scale, multi-room fire experiments. While the model was generally found to provide "favorable" simulations, several areas where improvements were needed were identified. They pointed out limitations in modeling of oxygen-limited burning, mixing of gases at vents, convective heat transfer, and plume entrainment. Deal [11] reviewed four computer fire models (CCFM, FIRST, FPETOOL [12] and FAST) to ascertain the relative performance of the models in simulating fire experiments in a small room. All the models simulated experimental conditions including temperature, species generation, and vent flows, "quite satisfactorily". Duong [13] studied the predictions of several computer fire models (CCFM, FAST, FIRST, and BRI), comparing the models with one another and with large fires in an aircraft hanger. For a 4 MW fire size, he concluded that all the models are "reasonably accurate". At 36 MW, however, "none of the models did well". Beard [14] evaluated four fire models (ASET, FAST, FIRST, and JASMINE [15]) by modeling three well-documented experimental fires, ranging in scope from the same tests used by Mitler and Rockett to a large-department-store space with closed doors and

windows. He provides both a qualitative and quantitative assessment of the models ability to predict temperature, smoke obscuration, CO concentration, and layer interface position (for the zone-based models). Peacock et al. [16] compared the CFAST model to a range of experimental fires. The model provided predictions of the magnitude and trends (time to critical conditions and general curve shape) for the experiments studied which range in quality from within a few percent to a factor of two or three of the measured values. Beck et al. [17] compared the NRCC fire growth model [18] to experiments with three types of fires and two compartment ventilation conditions. Comparisons of fuel burning rate, average compartment gas temperature, CO concentration and CO_2 concentration were presented. Model agreement between experimental and computational results was deemed "achieved in a qualitative sense". The model produced better estimates for fuel burning rate and average compartment gas temperature than for gas species concentrations. Björkman and Keski-Rahkonen [19] used the SOFIE CFD model [20] to predict conditions modeled after tests conducted by Steckler [21]. The model predicted conditions that matched well with experimental measurements. Velocities and temperatures in the compartment opening matched well with experimental measurements while temperatures inside the compartment were calculated 20–30°C higher than experimental measurements. Keski-Rahkonen [22] reviewed initial results of the CIB W14 round robin tests of a number of models used worldwide to predict conditions in the same test cases. Most of the variables studied were predicted within a factor of two. Davis et al. [23] compared model predictions with measured temperature profiles in the ceiling jet and fire plume using a range of fire models. Of the eight different comparisons made, the prediction of the plume centerline temperature was within 20% for four of the seven models studied. Model predictions of temperature and velocity within the ceiling jet were deemed much less satisfactory.

Common to nearly all of these comparisons is their qualitative nature. The level of agreement between the models and experiment is typically reported as "favorable", "satisfactory", "well predicted", "successful", or "reasonable". The intent of this study is to provide a more quantitative approach to making such comparisons. This will be done through the application of functional analysis to the comparison of fire model calculations and experimental data.

2. Functional analysis and simple vector math

Functional analysis is a generalization of linear algebra, analysis, and geometry. It is a field of study that arose around 1900 from the work of Hilbert and others. Functional analysis is becoming of increasing importance in a number of fields including theoretical physics, economics, and engineering to answer questions on differential equations, numerical methods, approximation theory, and applied mathematical techniques. Its power lies in its ability to take different ideas and apply a unified symbolism and theory with a strongly geometric flavor to deal with the important central features of the problem. In practice, functional analysis allows problems to be described in vector notation and defines operations on these vectors allowing

quantitative analysis of the properties of the underlying physical system. For this paper, the primary vector operations of interest are the norm, a measure of the length of a vector, and inner product, a measure of the angle between two vectors.

A simple sample of experimental data and a model prediction is shown in Fig. 1. A comparison of peak values at 60 s yields a difference of 6.9 or a relative difference, |experiment-model|/|experiment|, of 0.055.

While single-point comparisons are relatively easy to understand, comparing two time-dependent curves is considerably more difficult. In many instances, data is collected as a series of measurements over some time period. For the purposes of this paper, these data may be treated as a multi-dimensional set of vectors. In a one-dimensional space, the length of each vector is defined by the value of the data at that particular point with the sign of the value giving the vector direction. Angles in this space would be restricted to either 0 or 2π. For data sets, the simple comparison of the maxima for single points would evolve into finding the norm of the difference between the two vectors representing the data. In addition, a measure based on derivatives would be useful to quantify how well the shapes of the two curves match. For n data points, a multi-dimensional set of $n-1$ vectors can be defined to approximate the derivative as

$$x_i = \frac{x_{i+1} - x_i}{t_{i+1} - t_i}, \tag{1}$$

where, x_i is the measurement taken at time t_i. Since such differencing-based operations act like high-pass filters on the data, and can amplify jitter and transients present in

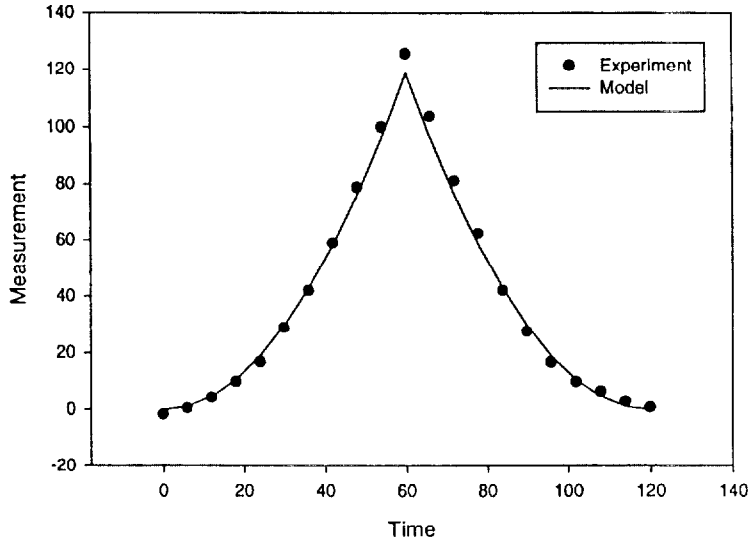

Fig. 1. Simple example of experimental data with accompanying model prediction.

the signal, smoothing techniques may be required to make the numerical derivatives useful.

2.1. Finding the length of a vector, the norm

The concept of a norm provides a definition of the length of a vector. The distance between two vectors is simply the length of the vector resulting from the difference of two vectors. The symbolic representation is written as $\|\boldsymbol{x}\|$ where $\boldsymbol{x}$ is the notation for the n-dimensional vector $(x_1, x_2, \ldots, x_{n-1}, x_n)$. As an extension of the comparison of maximum values, the norm based upon relative difference can be extended to multiple dimensions. A vector of values measured at each time point can represent all of the data, $\boldsymbol{E}$. A vector can also represent the model predictions at the same time points $\boldsymbol{m}$. The distance between these two vectors is the norm of the difference of the vectors, or $\|\boldsymbol{E} - \boldsymbol{m}\|$. It is convenient to normalize this as a relative difference to the experimental data as

$$\frac{\|\boldsymbol{E} - \boldsymbol{m}\|}{\|\boldsymbol{E}\|}. \tag{2}$$

The difference vector is calculated just as it was for the simple example comparing the maxima of the two curves, taking the difference between the experiment and model at each time point. The Euclidean norm takes the form

$$\|\boldsymbol{E} - \boldsymbol{m}\| = \sqrt{\sum_{i=1}^{n}(E_i - m_i)^2}. \tag{3}$$

where E_i and m_i are the ith experimental and model values. In statistics and curve-fitting, Eq. (3) represents the square root of the the residual sum of squares. The relative difference would be

$$\frac{\|\boldsymbol{E} - \boldsymbol{m}\|}{\|\boldsymbol{E}\|} = \sqrt{\frac{\sum_{i=1}^{n}(E_i - m_i)^2}{\sum_{i=1}^{n}(E_i)^2}}. \tag{4}$$

For the data of Fig. 1, the norm, $\|\boldsymbol{E} - \boldsymbol{m}\|$, is 14.1 and the relative difference is 0.056.

2.2. Finding the angle between two vectors, the inner product

While the difference, $\|\boldsymbol{E} - \boldsymbol{m}\|$, and the relative difference, $\|\boldsymbol{E} - \boldsymbol{m}\|/\|\boldsymbol{E}\|$, provide measures of the difference between experimental data and model predictions, other calculations provide useful information on the source of the difference. When comparing vectors, there are basically two geometric components to consider: a distance between the two vectors and an angle between the two vectors. The inner product, $\langle \boldsymbol{x}, \boldsymbol{y} \rangle$ of two vectors is the product of the length of the two vectors and the cosine of the angle between them, or

$$\langle \boldsymbol{x}, \boldsymbol{y} \rangle = \|\boldsymbol{x}\| \|\boldsymbol{y}\| \cos(\angle(\boldsymbol{x}, \boldsymbol{y})) \tag{5}$$

or

$$\cos(\angle(\boldsymbol{x},\boldsymbol{y})) = \frac{\langle \boldsymbol{x},\boldsymbol{y}\rangle}{\|\boldsymbol{x}\|\,\|\boldsymbol{y}\|}. \tag{6}$$

Choosing the inner product to be the standard dot product gives results consistent with typical Euclidean geometric perception

$$\langle \boldsymbol{x},\boldsymbol{y}\rangle = \sum_{i=1}^{n} x_i y_i. \tag{7}$$

For the vectors represented by the two curves of Fig. 1, $\cos(\angle(\boldsymbol{x},\boldsymbol{y})) \cong 1$. This angle between the two vectors represents a measure of how well the shape of the two vectors match. As the cosine of the angle approaches unity, the two curves represented by the two vectors differ only by a constant multiplier.

2.3. Properties of norms and inner products

Euclidean space is certainly not the only geometry that can provide a definition for the norm and inner product. In general, an inner product is simply a function that takes two vectors and returns a number. The number can be either real or complex. For our purposes, only real inner products will be considered. The following axioms provide a definition of the inner product and norm sufficient to have the necessary properties to perform vector calculations [24]:

	Inner product	Norm
I	$\langle \boldsymbol{x},\boldsymbol{x}\rangle \geqslant 0,$	$\|\boldsymbol{x}\| \geqslant 0,$
II	$\langle \boldsymbol{x},\boldsymbol{x}\rangle = 0 \Leftrightarrow \boldsymbol{x} = 0,$	$\|\boldsymbol{x}\| = 0 \Leftrightarrow \boldsymbol{x} = 0,$
III	$\langle \alpha\boldsymbol{x},\boldsymbol{y}\rangle = \alpha\langle \boldsymbol{x},\boldsymbol{y}\rangle,$	$\|\alpha\boldsymbol{x}\| = \|\alpha\|\|\boldsymbol{x}\|,$
IV	$\langle \boldsymbol{x}+\boldsymbol{y},\boldsymbol{z}\rangle = \langle \boldsymbol{x},\boldsymbol{z}\rangle + \langle \boldsymbol{y},\boldsymbol{z}\rangle,$	$\|\boldsymbol{x}+\boldsymbol{y}\| \leqslant \|\boldsymbol{x}\| + \|\boldsymbol{y}\|.$

For consistency, the norm can be defined in terms of the inner product. This ensures that appropriate, consistent definitions for the norm and inner product are used in calculations. Since the angle between a vector and itself is by definition zero, it follows from Eq. (5) that

$$\langle \boldsymbol{x},\boldsymbol{x}\rangle = \|\boldsymbol{x}\|^2 \text{ or } \|\boldsymbol{x}\| = \sqrt{\langle \boldsymbol{x},\boldsymbol{x}\rangle}. \tag{8}$$

With these properties and definitions of norms and inner products, additional useful comparisons of data can be made. For this paper, we will present three applications of these properties, discussed in the next sections.

2.4. Minimizing the difference between two vectors, the projection coefficient

One question that can be asked when comparing a model and an experiment is: is there a number, a, by which the model can be multiplied to give the smallest difference between the model and the experiment? The resulting vector, $a\boldsymbol{m}$, represents

the closest prediction the model can make to the chosen experiment without changing the functional form of the model. Solving for a is a minimization problem in the chosen norm, or

$$\text{solve}: \min \|a\boldsymbol{m} - \boldsymbol{E}\|. \tag{9}$$

From calculus, the minimum occurs when the derivative of the function is zero. To simplify, note that since the norm is non-negative the minimum of the norm occurs for the same value of a as the minimum of the squared norm. Using the definition of a norm in terms of the inner product and the rules for an inner product,

$$\begin{aligned}\|a\boldsymbol{m} - \boldsymbol{E}\|^2 &= \langle a\boldsymbol{m} - \boldsymbol{E}, a\boldsymbol{m} - \boldsymbol{E}\rangle \\ &= a^2\|\boldsymbol{m}\|^2 - 2a\langle \boldsymbol{m}, \boldsymbol{E}\rangle + \|\boldsymbol{E}\|^2.\end{aligned} \tag{10}$$

Since the norm and inner product are scalars, we can take the derivative with respect to a as

$$2a\|\boldsymbol{m}\|^2 - 2\langle \boldsymbol{m}, \boldsymbol{E}\rangle. \tag{11}$$

Finally setting the derivative equal to zero and solving for a gives

$$a = \frac{\langle \boldsymbol{m}, \boldsymbol{E}\rangle}{\|\boldsymbol{m}\|^2} = \frac{\|\boldsymbol{m}\|\,\|\boldsymbol{E}\|\cos\theta}{\|\boldsymbol{m}\|^2} = \frac{\|\boldsymbol{E}\|}{\|\boldsymbol{m}\|}\cos\theta. \tag{12}$$

For the purposes of this paper, a will be termed the projection coefficient. Geometrically, the vector $a\boldsymbol{m}$ is the projection of the vector $\boldsymbol{E}$ onto the vector $\boldsymbol{m}$ (Fig. 2). If the sign of the projection coefficient is positive, the angle between the two vectors is less than 90°; if the sign is negative, the angle is greater than 90°. If the magnitude of the projection coefficient is greater than 1, the model vector is smaller in magnitude than the experimental vector. The converse may or may not be true, depending upon the value of the cosine. For the example of Fig. 1, the projection coefficient is 1.05,

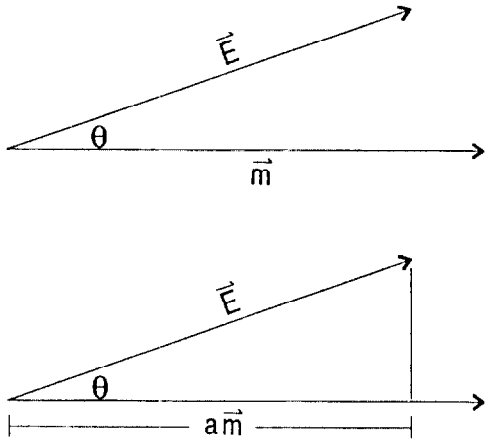

Fig. 2. The projection coefficient for two vectors.

indicating as expected, that increasing the model prediction by 5% would provide the closest (in this case, exact) model prediction for the fictitious experimental data. For real data, the projection coefficient would not lead to an exact match unless the functional form of the model is identical to the underlying form of the experimental data.

2.5. Other metrics

The properties for norms and inner products also provide appropriate rules to define the inner product and norm for other geometries in addition to Euclidean space. In this paper, two additional geometries, Hellinger and secant, will be investigated. Leigh et al. have proposed variants of these metrics for applications to coregistration and quantification of nonlinear correlation for matched two-dimensional time-varying curves [25,26].

The Hellinger inner product for functions x such that $x(0) = 0$ is defined based on the first derivative of the function

$$\langle x(t), y(t)\rangle = \int_0^T x'(t)y'(t)\,\mathrm{d}t. \tag{13}$$

For discrete vectors, this can be approximated with first differences as

$$\langle \boldsymbol{x}, \boldsymbol{y}\rangle = \sum_{i=2}^{n} \left(\frac{(x_i - x_{i-1})(y_i - y_{i-1})}{t_i - t_{i-1}} \right). \tag{14}$$

Based on the first derivative or tangents to the curves, the Hellinger inner product and norm provide a sensitive measure of the comparison of the shape of two vectors. A variation of the Hellinger inner product can be defined based on the secant rather than tangent as

$$\langle x(t), y(t)\rangle = \int_{pT}^{T} \frac{(x(t) - x(t - pT))(y(t) - y(t - pT))}{(pT)^2}\,\mathrm{d}t, \tag{15}$$

where T defines the time interval for integration and $0 < p \leqslant 0.5$ defines the length of the secant within this time interval. The limit of the secant inner product as $p \to 0$ is the Hellinger integral. For evenly spaced discrete vectors, this can be approximated analogous to the Hellinger geometry

$$\langle \boldsymbol{x}, \boldsymbol{y}\rangle = \sum_{i=s+1}^{n} \left(\frac{(x_i - x_{i-s})(y_i - y_{i-s})}{s^2(t_i - t_{i-1})} \right), \tag{16}$$

where s represents the number of data points in the interval. When $s = 1$, the secant definition is equivalent to the discrete Hellinger inner product. Depending on the value of p or s, the secant inner product and norm provide a level of smoothing of the data and thus better measures large-scale differences between vectors. For experimental data with inherent small-scale noise or model predictions with numerical instabilities, the secant provides a filter to compare the overall functional form of the curves without the underlying noise.

Appendix A contains the expressions necessary to calculate the norms and inner products for each of the three geometries.

3. Simple applications of functional analysis to data comparisons

To illustrate the use of the metrics in the comparison of time series data, this section will consider several examples of simple data sets and compare data from multiple curves using three measures. While these three measures are not the only ones that could be used to represent a comparison between two curves, they do provide a sufficient comparison for several areas important for the comparison of model predictions with experimental data.

- The norm based upon relative difference provides a measure of the difference in the overall magnitude for the two curves normalized to the experimental data. The norm based upon relative difference approaches zero when the two curves are identical in magnitude.
- The inner product cosine provides a comparison of the shapes of the two curves while minimizing the effect of small-scale variations in the data. The cosine approaches unity when the shapes of the two curves differ only by a constant multiplier.
- The projection coefficient provides a measure of the best possible fit of the two curves. When the projection coefficient approaches unity, remaining differences between the two curves is either due to random noise in the experimental measurements or physical effects not included in the model.

Fig. 3 shows a second simple example of fictitious experimental data compared with three model predictions. Model 1 is simply the experimental data multiplied by 0.9. Model 2 has the same peak value as model 1, but with the peak shifted – 25 s. Model 3 has the same peak as Models 1 and 2, but with a 20 s plateau centered around the peak of the experimental data. The comparison only of maxima would show that all three models are identical with a relative difference of 0.1. Clearly this comparison fails to capture the differences between the three models. Table 1 shows the relative difference, cosine, and projection coefficient between the vectors of experimental data and model predictions for the three models using other definitions for the inner product and norm.

All of the geometries rank the models in the same order, with Model 1 closest to the experimental data, followed by Models 3 and 2. The rank order matches a visual interpretation of the comparisons. Model 1 is clearly the best, with the same functional form (cosine = 1) and a projection coefficient close to one. The relative difference for Model 1 is the same for all of the geometries as it should be. By choice, the vector form of Model 1, $\boldsymbol{m}$, is simply $\boldsymbol{m} = 0.9\boldsymbol{E}$. Thus, the relative difference, $\|\boldsymbol{E} - \boldsymbol{m}\|/\|\boldsymbol{E}\|$, regardless of the definition of the norm is just $\|\boldsymbol{E} - 0.9\boldsymbol{E}\|/\|\boldsymbol{E}\|$ or 0.1. Similarly, the cosine of the angle between Model 1 and the experiment is 1.0 for all of the comparisons. This is expected from axiom III for the inner product where one data set is related to a second data set by a constant multiplier.

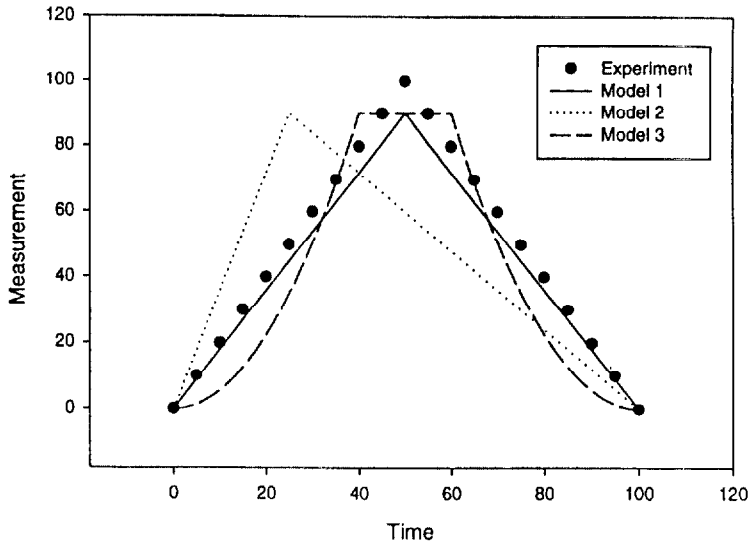

Fig. 3. Three possible model predictions for a fictional example of experimental data.

Table 1
Comparison of fictional experimental data with three model predictions using several different inner product definitions

	Model	Relative difference	Cosine	Projection coefficient
Euclidean	1	0.10	1.00	1.11
	2	0.40	0.92	1.02
	3	0.20	0.98	1.05
Hellinger	1	0.10	1.00	1.11
	2	0.94	0.58	0.56
	3	0.74	0.77	0.67
Secant	1	0.10	1.00	1.11
	2	0.92	0.58	0.57
	3	0.66	0.83	0.71

Conversely, Model 2, with its peak offset from the experimental peak yields a Euclidean projection coefficient close to one, but the difference in slope is clearly shown in the cosine for the Hellinger and secant geometries. Although Model 3 does not have the correct type of peak (an elongated plateau rather than a sharp peak), it does have the right general form. These may be compared with the results of Model 2. The projection coefficient is slightly larger for Model 3, but the value of the cosine moved closer to one indicating that the shape of Model 3 is a better fit than Model 2.

The Euclidean model provides a straightforward means for measuring relative difference that can be related to experimental and model uncertainties. The Euclidean

cosine calculation is less useful since it is not based on the first derivative and therefore does not provide a sensitive measure of curve shape. For example, two curves with the same slope but offset by a constant amount compared to a third curve (Fig. 4) yield different values for the cosine using the Euclidean geometry (0.36 and 0.55 for curves 1–2 and 1–3, respectively. The Hellinger and secant geometries yield the same cosine values for curves 1–2 and 1–3 (0.25 and 0.41 for the Hellinger and secant, respectively).

A norm calculated in the Hellinger geometry would be a norm for the first derivatives of the curve and not for the curve. This would make using the norm difficult to relate back to experimental uncertainty. A practical drawback to this method is that for noisy data, the cosine representation would have a substantial contribution from the shape of the noise and would not provide a good representation for the overall curve shape. The secant geometry is a variation of the Hellinger geometry that is designed to reduce or filter the noise contribution to the calculations. This is accomplished by requiring that the derivative be taken over a number of data points rather than adjacent points as in the Hellinger case. The difficulty of relating the norm to data uncertainty has the same problems as the Hellinger method. The choice of smoothing interval will effect the value of the cosine as the curve is effectively being replaced by a series of chords.

Fig. 5 shows two curves compared to a straight line. For one of the curves, a dotted line shows the curve with a $\pm$ 5% random error. For the two experimental curves, the Hellinger geometry yields cosine values of 0.90 and 0.87; the secant geometry values of 0.94 and 0.90. Introducing the 5% error to experiment 1 drops the Hellinger value to 0.81, but leaves the secant value nearly unchanged.

For a comparison method to be useful, it should be sensitive, easily interpreted, and measure the proper characteristics. For the comparisons given later in the paper, the

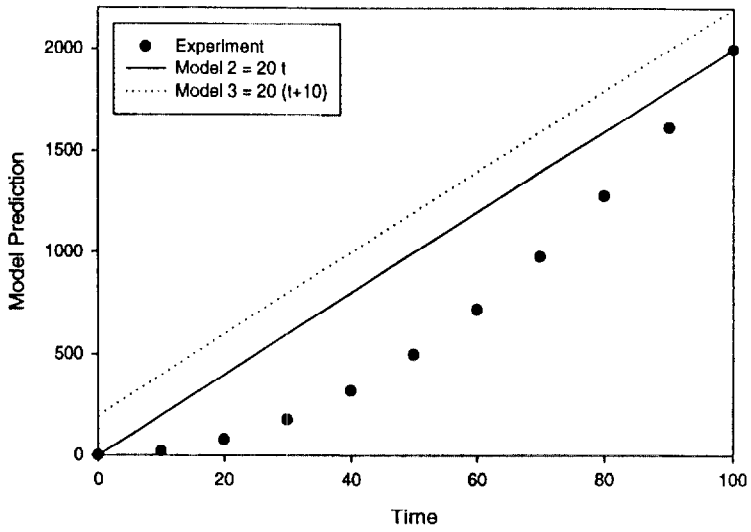

Fig. 4. Comparison of curve magnitude.

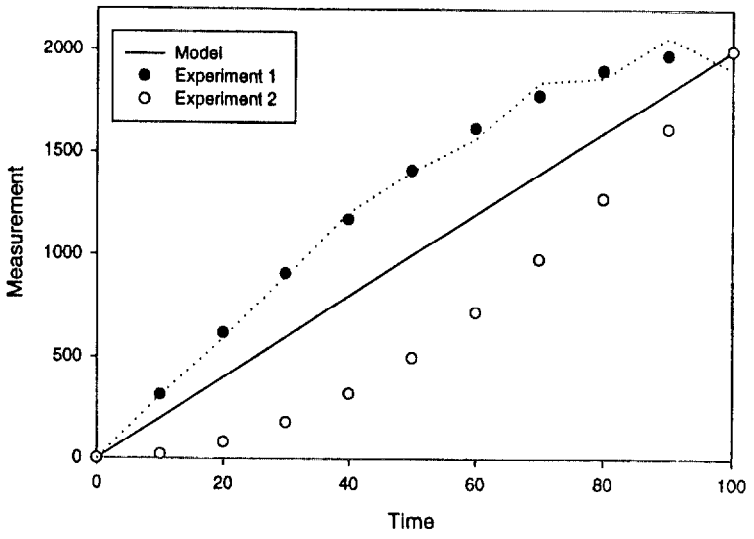

Fig. 5. Comparison of curve shape.

Euclidean geometry will be used to calculate the norms and the secant geometry will be used to calculate the cosines. The Euclidean norm provides both a straightforward interpretation and a measure of average curve separation that could be related to data uncertainties. The secant inner product cosine was chosen based on its noise handling ability and because it provides a measure of curve shapes which was based only on first derivatives of the two curves. The resulting cosine would be relatively easy to interpret compared with the other methods.

4. Quantifying the comparison of model predictions with experimental data

Most of the studies in the literature present a consistent set of variables of interest to the model user: gas temperature, gas species concentrations, and layer interface position. To assess the accuracy of the physical basis of the models, additional variables must be included. Pressure drives the movement of gases through openings. The pyrolysis rate and heat release rate of the fire in turn produces the gases of interest to be moved. Peacock et al. [16] compared the performance of the CFAST model with experimental measurements for these variables. Using a range of laboratory tests, they presented comparisons of peak values, average values, and overall curve shape for a number of variables of interest to model users. Details of the geometry, experimental measurements, and model predictions are available [16].

A selection of data from one of these tests (a single-compartment test) will be used in this paper to provide examples of comparisons quantified using the norm and inner product. Table 2 presents the Euclidean relative difference, secant inner product cosine, and Euclidean projection coefficient for a selection of the data from a single

Table 2
Relative difference, cosine, and projection coefficient for a single room test

	Relative difference	Cosine	Projection coefficient
Upper layer temperature	0.18	0.99	1.08
	0.26	0.97	1.01
Lower layer temperature	0.46	0.95	1.56
	0.38	0.93	1.03
Interface position	1.40	−0.72	−1.45
	0.54	0.85	1.15
Heat release rate	0.10	1.00	1.03
Oxygen concentration	0.35	0.95	1.23
Carbon dioxide	0.64	0.97	2.54
Carbon monoxide	0.86	0.83	4.60
Vent flow	0.58	0.84	1.29

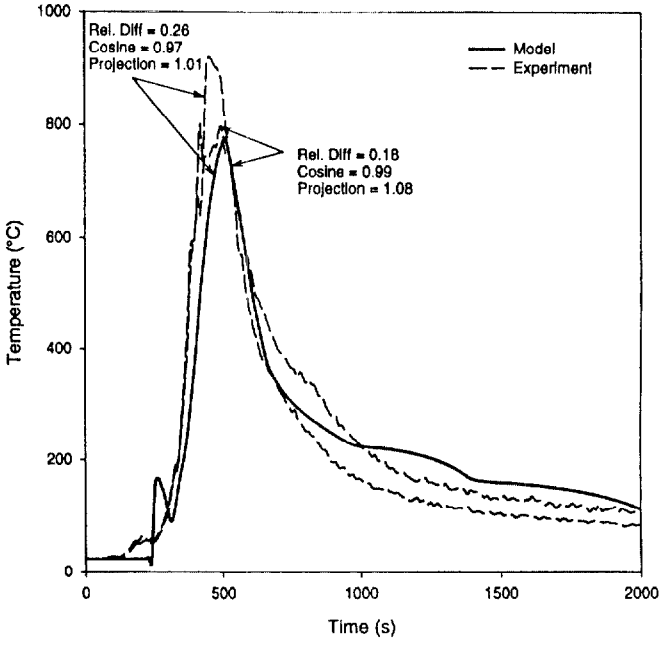

Fig. 6. Comparison of upper layer temperature for a single-room test.

compartment test. To better understand these quantified comparisons, Figs. 6–8 present both the experimental data and model predictions for several of the variables included in Table 2. All of the experimental data were collected at 10 s intervals. For the secant inner product cosine, a value of s of 5 was used to provide appropriate noise filtering for the experimental data.

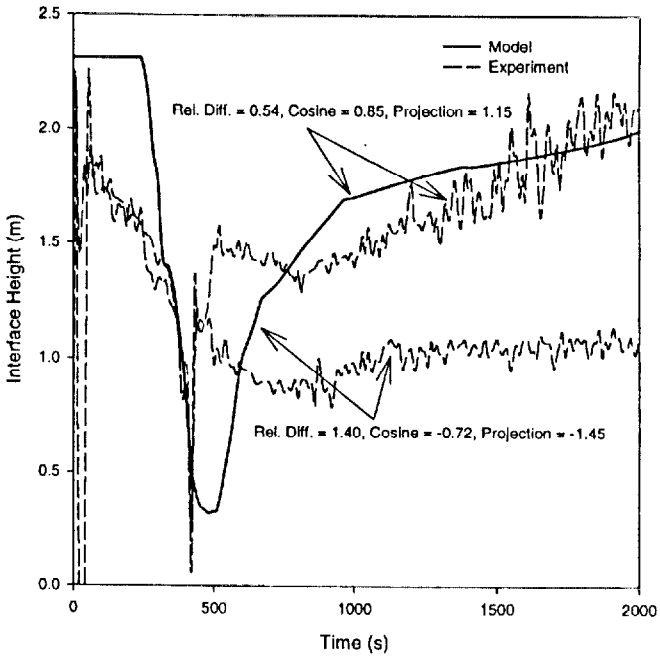

Fig. 7. Comparison of layer interface position for a single-room test.

Fig. 6 shows a comparison of upper layer temperatures for a single room test. In this test, two measurement positions were available from the experimental data. The predicted temperatures show obvious similarities to the measured values. Peak values occur at similar times with comparable rise and fall for both measurement positions. For both positions, the rise in upper layer temperatures is faster than the model predictions. Both the relative difference and cosine reflect these trends. The norm based upon relative difference is somewhat higher for one of the experimental positions (0.26 versus 0.18) reflecting the higher temperature at this measurement position. With the shapes of all the curves similar, the cosine shows similar values for the two comparisons (0.99 and 0.97). With both the magnitude and curve shape similar for the two comparisons, the projection coefficient is close to unity for both curves.

The relative difference and cosine for the comparison of interface position and vent flow for this same test also reflect trends in the data. Fig. 7 shows the interface position calculated from experimental temperature profiles compared with that predicted by the CFAST model. For one of the measurement positions, the dip in the layer height from 2 to 1 m at about 500 s is evident in both the experimental measurements and in the model prediction. The relative difference, cosine, and projection coefficient for this comparison are 0.58, 0.85 and 1.15, respectively. For the other measurement position, the interface height drops to about a 1 m height and remains there for the duration of the test. A higher relative difference of 1.40 and negative values for the cosine and projection coefficient of -0.72 and -1.45 reflect the larger differences at this

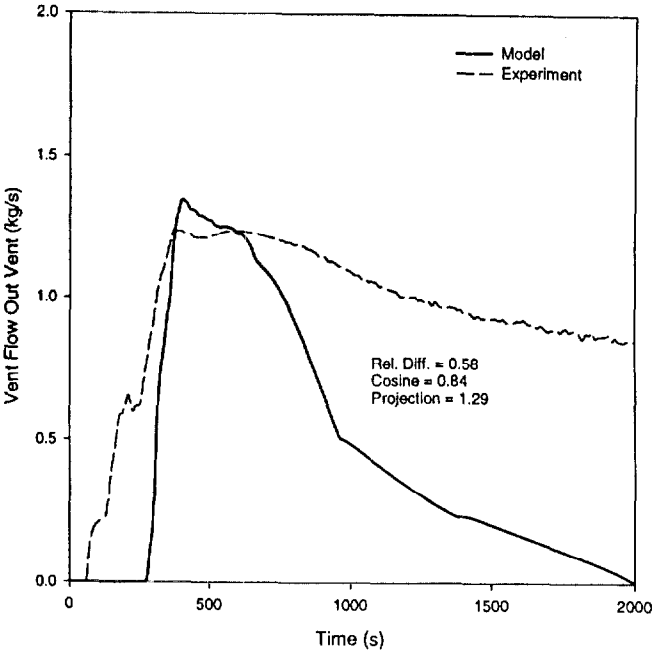

Fig. 8. Comparison of vent flow for a single-room test.

measurement position. For both positions, the cosine values are lower than those of the upper layer temperature comparisons due both to differences in the shapes of the curves and to high noise in the experimentally determined interface position.

Fig. 8 shows the vent flow calculated from measured pressure profiles in the doorway of the room compared with that predicted by the CFAST model. The relative difference, cosine, and projection coefficient for this comparison are 0.58, 0.84 and 1.29, respectively. The experiment and model prediction rising and falling over similar times are reflected in the cosine value of 0.84. The relative difference and projection coefficient values reflect the significantly lower model predictions in the latter part of the test.

5. Summary

In the past, the comparison of experimental measurements with model predictions has been largely qualitative in nature. This paper has proposed techniques that allow quantification of the differences between experimental measurements and model predictions in the context of zone fire modeling. Several areas in need of further examination are apparent:

- The techniques presented in this paper provide comparisons of magnitude and functional form consistent with visual examination of the comparisons. However,

these are based on a limited set of data. Additional comparisons are necessary to build confidence that the techniques are chosen to best match visual perceptions of model performance.

- In addition to comparison with experimental data, tests of the techniques with simple examples would provide a better understanding of the limits of the comparisons.
- In addition to fire model comparisons, the techniques should also be applicable to other areas of interest to researchers. Application to sensitivity analysis, time shifting of data curves for optimal matching of ignition time and adaptive modeling are similar to those presented in this paper.

Additional analysis and comparison with a wider range of applications is appropriate to provide a better understanding of the use of functional analysis in fire safety analyses.

Appendix A. Calculation of the norm and inner product

Detailed equations are presented in this appendix for the calculation of the norm and the inner product in the Euclidean, Hellinger and secant vector spaces. The Euclidean norm is calculated using

$$\frac{\|E-m\|}{\|E\|}=\frac{\sqrt{\sum_{i=1}^{n}(E_i-m_i)^2}}{\sqrt{\sum_{i=1}^{n}(E)_i^2}},$$

while the inner product is given by

$$\frac{\langle E,m\rangle}{\|E\|\,\|m\|}=\frac{\sum_{i=1}^{n}E_i m_i}{\sqrt{\sum_1^n E_i^2\sum_1^n m_i^2}}.$$

Here E_i and m_i represent the ith experimental and model data points in a set of n points.

The Hellinger norm is calculated using

$$\frac{\|E-m\|}{\|E\|}=\frac{\sqrt{\sum_{i=2}^{n}[(E_i-E_{i-1})-(m_i-m_{i-1})]^2/(t_i-t_{i-1})^2}}{\sqrt{\sum_{i=2}^{n}(E_i-E_{i-1})^2/(t_i-t_{i-1})}},$$

while the inner product is given by

$$\frac{\langle E,m\rangle}{\|E\|\,\|m\|}=\sum_{i=2}^{n}\frac{(E_i-E_{i-1})(m_i-m_{i-1})}{(t_i-t_{i-1})}\Bigg/\sqrt{\sum_{i=2}^{n}\frac{(E_i-E_{i-1})^2}{(t_{i+1}-t_i)}\sum_{i=2}^{n}\frac{(m_i-m_{i-1})^2}{(t_i-t_{i-1})}}.$$

The secant norm and inner product are similar to the Hellinger norm and inner product with the exception that the sums are taken over an interval s which is a method to smooth noisy data. If short period oscillations with a period equivalent to a few data points are superimposed on a data signal, then by picking an interval s which is larger than the oscillation interval provides a data smoothing effect and the

impact of the short period oscillations on the data analysis will be lessened. The secant norm and inner product are given by

$$\frac{\|E-m\|}{\|E\|}=\frac{\sqrt{\sum_{i=2}^{n}[(E_i-E_{i-s})-(m_i-m_{i-s})]^2/(s^2(t_i-t_{i-1}))}}{\sqrt{\sum_{i=2}^{n}(E_i-E_{i-1})^2/(s^2(t_i-t_{i-1}))}}$$

and

$$\frac{\langle E,m\rangle}{\|E\|\,\|m\|}=\frac{\sum_{i=2}^{n}(E_i-E_{i-s})(m_1-m_{i-s})/(t_i-t_{i-1})}{\sqrt{\sum_{i=2}^{n}(E_i-E_{i-s})^2/(s^2(t_i-t_{i-1}))\sum_{i=2}^{n}(m_i-m_{i-s})^2/(s^2(t_i-t_{i-1}))}}$$

References

[1] Standard Guide for Evaluating the Predictive Capability of Fire Models, ASTM E 1355-97, Annual book of ASTM standards, Vol. 04.07. Philadelphia: American Society for Testing and Materials, 1998.

[2] Standard Guide for Guide for Documenting Computer Software for Fire Models, ASTM E 1472, Annual book of ASTM standards, Vol. 04.07. Philadelphia: American Society for Testing and Materials, 1995.

[3] Forney GP, Moss WF. Analyzing and exploiting numerical characteristics of zone fire models. Fire Sci Technol 1994;14(1/2):49–60.

[4] Nelson HE. An engineering view of the fire of May 4, 1988 in the First Interstate bank building, Los Angeles, California. Natl Inst Stand Technol NISTIR 89-4061, 1989. 39 pp.

[5] Bukowski RW. Reconstruction of a fatal residential fire at Ft. Hood, Texas. First HAZARD I Users' Conference, National Institute of Standards and Technology, Gaithersburg, MD, June 5–6 1990.

[6] Bukowski RW. Analysis of the Happyland social club fire with HAZARD I. Fire Arson Investigator 1992;42(3):36–47.

[7] Bukowski RW. Modeling a backdraft: the fire at 62 Watts Street. NFPA J 1995;89(6):85–9.

[8] Emmons HW. Why fire model? The MGM fire and toxicity testing. Fire Safety J 1988;13:77–85.

[9] Mitler HE, Rockett JA. How accurate is mathematical fire modeling? Nat Bur Stand (U.S.). NBSIR 86-3459, 1986, 50 pp.

[10] Rockett JA, Morita M, Cooper LY. Comparisons of NBS/HARVARD VI simulations and data from all runs of a full-scale multi-room fire test program. Fire Safety J 1989;15:115–69.

[11] Deal S. A review of four compartment fires with four compartment fire models. Fire safety developments and testing. Proceedings of the Annual Meeting of the Fire Retardant Chemicals Association. October 21–24, Ponte Verde Beach, Florida, 1990. pp. 33–51.

[12] Nelson HE. FPETOOL: fire protection engineering tools for hazard estimation. Natl Inst Stand Technol NISTIR 4380, 1990. 120 pp.

[13] Duong DQ. The accuracy of computer fire models: some comparisons with experimental data from Australia. Fire Safety J 1990;16(6):415–31.

[14] Beard A. Evaluation of fire models: overview. Unit of Fire Safety Engineering, University of Edinburgh, Edinburgh, UK, 1990.

[15] Cox G, Kumar S. Field modeling of fire in forced ventilated enclosures. Combust Sci Technol 1987;52:7–23.

[16] Peacock RD, Jones WW, Bukowski RW. Verification of a model of fire and smoke transport. Fire Safety J 1993;21:89–129.

[17] Beck V, Yung D, He Y, Sumathipala. Experimental validation of a fire growth model. Proceedings of interflam 96, Seventh International Fire Science and Engineering Conference. March 26–28, Cambridge, England, 1996. pp. 653–62.

[18] Takeda H, Yung D. Simplified fire growth models for risk-cost assessment in apartment buildings. J Fire Prot Engr 1992;4(2):53–66.

[19] Björkman J, Keski-Rahkonen, O. Simulation of the Steckler room fire experiment by using SOFIE CFD-model. VTT – Technical Research Centre of Finland, VTT-PUBS-265, 1996.
[20] Cox G, Rubini PA. Development of a new CFD fire simulation model. Proceedings of the Nordic Fire Safety Engineering Symposium. Development and Verification of Tools for Performance Codes. August 30–September 1, Espoo, Finland, 1993. pp. 1–11.
[21] Steckler KD, Quintiere JG, Rinkinen WJ. Flow induced fire in a compartment. Nineteenth Symposium (international) on Combustion. The Combustion Institute, Pittsburgh, 1982. pp. 913–20.
[22] Keski-Rahkonen O. CIB W14 Round Robin for code assessment, a comparison of fire simulation tools. Procedings of the Open Symposium on Fire Safety Design of Buildings and Fire Safety Engineering.
[23] Davis WD, Notarianni KA, McGrattan KB. Comparison of fire model predictions with experiments conducted in a hangar with a 15 meter ceiling. Natl Inst Stand Technol NISTIR 5927, 1996. 64 pp.
[24] Kreyszig E. Introductory functional analysis with applications. New York: Wiley, 1989. pp. 63–4.
[25] Leigh S, Perlman S, Rukhin A. A comovement coefficient for time sequences, in review.
[26] Ramsay JO, Silverman BW. Functional data analysis. New York: Springer, 1996. pp. 67–83.